SCIENCE CHINA
Information Sciences

• LETTER •

October 2021, Vol. 64 209303:1–209303:2
https://doi.org/10.1007/s11432-020-3165-8

Design of low-profile array antenna working at 110 GHz based on digital coding characterization

Qiang WANG, Weixiang JIANG* & Haiyang SHEN

State Key Laboratory of Millimeter Waves, Department of Radio Engineering, Southeast University, Nanjing 210096, *China*

Received 5 July 2020/Revised 18 December 2020/Accepted 4 January 2021/Published online 7 September 2021

Citation Wang Q, Jiang W X, Shen H Y. Design of low-profile array antenna working at 110 GHz based on digital coding characterization. Sci China Inf Sci, 2021, 64(10): 209303, https://doi.org/10.1007/s11432-020-3165-8

Dear editor,

Metasurfaces have been proposed and investigated in the past years owing to their unique advantages in controlling electromagnetic (EM) waves. By adjusting the phase and amplitude of EM waves, we can achieve the desired functions based on metasurfaces [1]. In 2014, the digital coding metasurfaces were proposed by Cui et al. [2]. In such a method, the phase response of metasurface is characterized by digital bits [3]. To satisfy the requirements of the high data rate and adaptive communication with beamforming ability, higher operation frequencies with large bandwidth are used as wireless communication frequencies, especially in millimeter-waves (mmW) and Terahertz (THz) regions [4,5]. However, affected by processing and parasitic effects, it is hard to extend the performance to higher frequencies for the tunable devices with common semiconductor components adopted in the microwave band. Hence, researchers started to look for new phase-changing techniques based on the characteristics of different materials, such as liquid crystal, graphene, and VO_2 [6]. In particular, it is found that the nematic liquid crystals (NLCs) have a unique response to EM waves in the THz frequency band with the merits of low loss, and facility of integration.

In this study, we propose and design a mmW array antenna operating at 110 GHz based on digital coding characterization and NLCs for future wireless communication. The array antenna is composed of NLCs antenna units arranged in period to achieve dynamic beams canning, beam switching, and high gain. The antenna unit structure has the advantages of ultra-low profile ($0.067\lambda_0$) and high-frequency phase tunability (2π), and can be used in a large-scale array. A 1-to-16 power divider network is designed to route EM signals to the coupling structure beneath each antenna unit, thereby forming a 4×4 array antenna. 1-bit dual-beam scanning and 3-bit single-beam scanning are realized by such an array antenna.

To realize an NLC array antenna (Figure 1(a)) working at 110 GHz based on digital coding technology, we first design the antenna unit based on NLCs to obtain full phase coverage. The detailed geometry structure of the antenna unit is illustrated in Figure 1(b). The unit, from top to bottom, is composed of 6 layers, which are radiation patch layer, upper glass substrate, ground plane and slot, NLCs, inverted microstrip lines (IMSL), and bottom glass substrate. The radiation element is a sub-wavelength square patch with side-length $0.2\lambda_0$ at 110 GHz. The material parameters of NLCs are provided by Merck, and the dielectric constant varies from 2.4 to 3.2 by tuning direct-current (DC) voltage, and the tangent loss is 0.005. The radiation elements, ground and IMSL are photoetched on a typical substrate of silicon glass (BF33), for which the permittivity and loss tangent are 4.65 and 0.001 at the operating frequency, respectively. The radiation element is fed by the coupling slot, with the size $L_a \times L_b$. In addition, the spiral structure of phase shifter can greatly save the occupied space, and the input impedance is 50 Ohm and the line width is set up as w_s. The thicknesses of silicon glass dielectric substrates, NLCs materials and metal copper are H_s, $H_{\rm LC}$ and t, respectively. The optimized geometry parameters of the antenna unit and simulated results are shown in Appendix A. Note that the metal thickness is five times larger than the skin effect depth at the designed frequency, and therefore, EM wave cannot penetrate the metal. The antenna unit works at 110 GHz frequency with 6 dBi gain and the radiation patterns in E-plane and H-plane are almost coincident.

A 1-to-16 ways power divider containing quarter-wave ($L_g = 0.43$ mm) stubs is designed as a feeding network to provide equal-amplitude in-phase EM wave signals for each antenna unit. The Chebyshev impedance distribution is implemented in the design of the feeding network to ensure the transmission of EM signal and couple to the upper antenna units. To reach 50 Ohm, we calculate the width of the microstrip line w_0, w_1 by using the software, advanced design system (ADS). We select one quarter-wavelength branch for impedance matching in the working band of the feeding network. The width and length of the microstrip are optimized as, $w_0 = 0.015$ mm, $w_1 = 0.025$ mm. The antenna unit is optimized to match its input impedance. The structure of the power divider network is shown in Figure 1(c). Note that, the corners of the microstrip lines in the power divider network are sheared to avoid unwanted reflections and achieve

* Corresponding author (email: wxjiang81@seu.edu.cn)

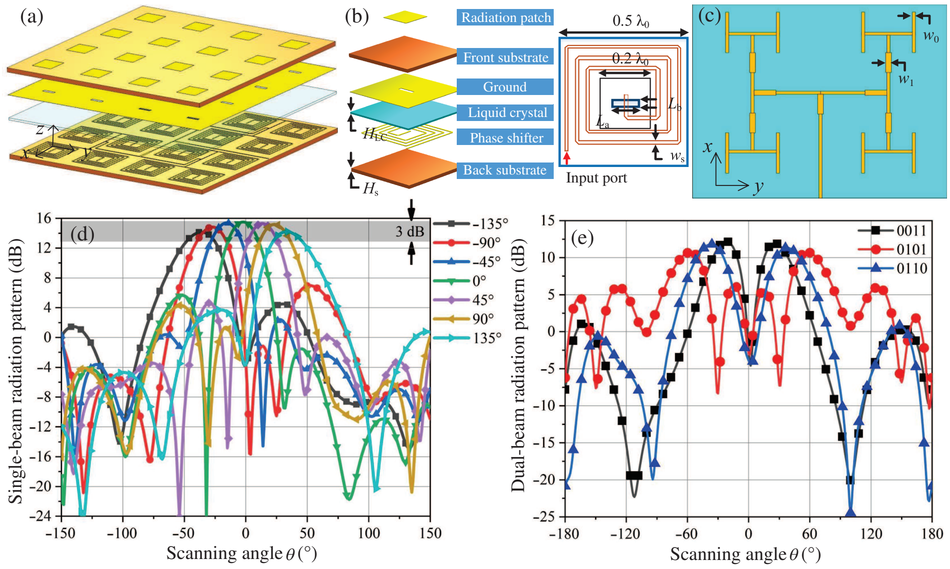

Figure 1 (Color online) Low-profile array antenna working at 110 GHz. (a) Illustration of array antenna based on NLCs; (b) geometries of the antenna unit; (c) the power divider network; (d) simulated single-beam scanning results of 3-bit array antenna; (e) simulated dual-beam scanning results of 1-bit array antenna.

a wideband impedance matching, as shown in Appendix A.

We arrange the units to compose an array antenna and obtain the desired radiation pattern with high gain. The orientation of each NLCs molecular can be rotated by varying the bias voltage, resulting in the adjustment of the relative permittivity. The antenna units are assigned in a 4×4 periodic array, as shown in Figure 1(a). S_{11} of the array antenna is less than -20 dB at the operating frequency, which is shown in Appendix B. Since the coupling between the antenna unit and the feeding branch, the operating frequency is shifted from 110 to 111 GHz.

We character the NLCs array antenna based on the digital coding method, hence, the EM beams can be controlled through a small number of discrete phase states. Generally, the discrete phase states for N-bits can be expressed by $360^\circ/2^N$. High phase accuracy can be realized by using more digital coding bits, which is helpful for achieving further EM wave functions. For example, a 3-bit phase discrete coding distribution can realize 8 different phase changes, including all the states of 1-bit and 2-bit coding.

We simulate the beam scanning performances of the array antenna working at 110 GHz. Figure 1(d) shows the single-beam scanning results of a 3-bit coding array antenna, and the scanning angle θ covers from -40° to 40°. The relationship between the one-dimensional scanning angle of the array antenna and the dielectric constant of the NLCs is listed in Appendix C. To achieve a larger phase tuning in a small physical area, we design the helical-structure phase shifter to feed the antenna patch. The helical-structure phase shifter causes some losses, especially in THz band. In addition, the designed 1-to-16 power divider also loses some EM energy. Therefore, the total gain of the 3-bit coding antenna array is 15.7 dBi. The calculational scanning angle θ related to the phase difference $\Delta\phi$ can be expressed as

$$\theta = \arcsin\left(\frac{\Delta\phi\lambda}{2\pi d}\right), \tag{1}$$

where λ is the wavelength in free space, and d is the period of antenna units.

Based on the 1-bit digital coding array antenna, a dual-beam radiation can be realized simply. Here, the 1-bit phase states are carried out by varying the dielectric constant of NLCs. The dual beams can cover a larger communication range and realize multi-sector communication. We simulate three sequences of 0011, 0101, 0110 for dual-beam scanning. It is observed from Figure 1(e), that the maximum gain of the dual-beam is 12.1 dBi, and the scanning range covers from -22° to -57°. The single-beam and dual-beam scanning modes can be freely switched by adjusting the bias voltage loaded on the NLCs, and the scanning mode can also be freely adjusted according to the actual needs of communication. The response time of the liquid crystal used in this study is about several milliseconds.

In this study, we proposed, designed and verified a low-profile digital coding array antenna based on NLCs. This array antenna supports electrical reconfigurability and massive intelligent operation for future wireless communications.

Acknowledgements This work was supported by National Ten-Thousands Talents Plan and National Natural Science Foundation of China (Grant No. 61890544).

Supporting information Appendixes A–C. The supporting information is available online at info.scichina.com and link.springer.com. The supporting materials are published as submitted, without typesetting or editing. The responsibility for scientific accuracy and content remains entirely with the authors.

References

1 Yu N F, Genevet P, Kats M A, et al. Light propagation with phase discontinuities: generalized laws of reflection and refraction. Science, 2011, 334: 333–337
2 Cui T J, Qi M Q, Wan X, et al. Coding metamaterials, digital metamaterials and programmable metamaterials. Light Sci Appl, 2014, 3: e218
3 Zhang X G, Jiang W X, Jiang H L, et al. An optically driven digital metasurface for programming electromagnetic functions. Nat Electron, 2020, 3: 165–171
4 Wang Q, Zhang X G, Tian H W, et al. Millimeter-wave digital coding metasurfaces based on nematic liquid crystals. Adv Theor Simul, 2019, 2: 1900141
5 Fan Y C, Shen N H, Zhang F L, et al. Photoexcited graphene metasurfaces: significantly enhanced and tunable magnetic resonances. ACS Photonics, 2018, 5: 1612–1618
6 Kim Y, Wu P C, Sokhoyan R, et al. Phase modulation with electrically tunable vanadium dioxide phase-change metasurfaces. Nano Lett, 2019, 19: 3961–3968